Thermoelectric and thermal stability improvements in Nano-Cu$_2$Se included Ag$_2$Se

Sedat Ballikaya [a,*], Yildirhan Oner [b], Tugba Temel [c], Burak Ozkal [c], Trevor P. Bailey [d], Muhammet S. Toprak [e], Ctirad Uher [d]

[a] Physics Department, Istanbul University, Fatih, 34134, Turkey
[b] Department of Physics Engineering, Istanbul Technical University, Maslak, Istanbul, Turkey
[c] Metallurgical and Materials Engineering Department, Istanbul Technical University, Maslak, 34469 Istanbul, Turkey
[d] Department of Physics, University of Michigan, Ann Arbor, MI, 48109, USA
[e] Department of Applied Physics, KTH Royal Institute of Technology, SE10691, Stockholm, Sweden

ABSTRACT

Recently, silver chalcogenides have attracted great attention due to their potential application for room temperature power generation and local cooling. In this work, we report the thermoelectric properties and thermal stability of bulk Ag$_2$Se with nano-Cu$_2$Se inclusions ((Ag$_2$Se)$_{1-x}$(Cu$_2$Se)$_x$ where x = 0, 0.02 and 0.05). Ag$_2$Se samples were prepared via melting, annealing and the nanocomposite was prepared by ball milling this material with required amount of nano-Cu$_2$Se; finally, the samples were consolidated by spark plasma sintering. High temperature and low temperature transport properties were assessed by the measurements of the Seebeck coefficient, electrical conductivity, thermal conductivity, and Hall coefficient. The phase composition and microstructure were explored by powder X-ray diffraction (PXRD) and scanning electron microscopy (SEM) with energy dispersive X-ray (EDX) analysis, while the thermal stability of samples was investigated via heating microscopy and heat capacity measurement. Room temperature PXRD and SEM indicated that two separate phases of Ag$_2$Se and Cu$_2$Se form in nano-Cu$_2$Se included composites. Heating microscopy and the heat capacity measurement indicate that the thermal stability of Ag$_2$Se is enhanced with increasing nano-Cu$_2$Se inclusions. The sign of the Seebeck coefficient, in agreement with the Hall coefficient, shows that electrons are the dominant carriers in all samples. The electrical conductivity of the samples increases and the Seebeck coefficient decreases with increasing amount of the nano-Cu$_2$Se inclusion, likely due to augmented carrier concentration. Despite the larger electrical conductivity, the thermal conductivity is suppressed with nano-Cu$_2$Se inclusions. A high power factor and reduced thermal conductivity lead to a maximum ZT value of 0.45 at 875 K for (Ag$_2$Se)$_{1-x}$(nano-Cu$_2$Se)$_x$ sample where x is 0.05.

1. Introduction

Today almost 60% of world energy use globally is rejected to the atmosphere as waste heat, much of it coming from automobiles and industrial settings [1]. Thermal-to-electric power conversion via thermoelectric (TE) materials is one of the most promising technologies to convert a part of this energy to useful electric power [2,3]. TE materials are capable of converting heat energy directly into electricity, and vice versa, with very little maintenance, noiseless operation and fully solid-state means. The efficiency of a TE material is determined by the TE figure of merit, Z. Its dimensionless form, ZT, is characterized by three parameters, $ZT = S^2\sigma T/\kappa$ where S, σ, and κ are the Seebeck coefficient,

electrical conductivity, and total thermal conductivity ($\kappa = \kappa_e + \kappa_L$ where κ_e is the electronic contribution and κ_L the lattice contribution), respectively, and T is the absolute temperature. An ideal TE material should have a high power factor ($S^2\sigma$) as well as low thermal conductivity. However, because of the interrelation between transport parameters, it is very challenging to achieve high ZT values > 2 in bulk materials. A general method to design a TE material with high ZT is to select an extrinsic semiconductor with good electronic properties (high charge carrier mobility) and attempt to reduce its thermal conductivity as much as possible. In recent years, several novel approaches, such as the Phonon-Glass-Electron-Crystal (PGEC) paradigm [4,5], formation of bulk nanocomposite structures [6,7], the use of electronic energy band

resonant states [8], composition and temperature induced band convergence [9,10], seeking materials with extremely unharmonic lattice vibrations [11], using ultra-fast solidification techniques [12], the Phonon-Liquid-Electron-Crystal (PLEC) concept [13,14] and even synergetic band engineering have been implemented to enhance the efficiency of TE materials [15]. Among the TE families, chalcogenides such as PbTe, alloys of PbTe and $AgSbTe_2$ (called LAST materials), alloys of GeTe and $AgSbTe_2$ (called TAGS), Bi_2Te_3, Cu_2Se, and Ag_2Se have been widely studied due to their high electrical conductivity and low thermal conductivity [6,16,17]. In particular, n-type $Ag_{2+x}Se$ is a known superionic compound [18], similar to Cu_2Se, with an alpha (α) to beta (β) phase transition around 400 K through which the crystal structure turns from the orthorhombic α-phase to the cubic superionic β-phase [19]. The small electronic energy band gap of Ag_2Se (~0.20 eV) leads to easy modification of the transport properties for different applications [19–22]. The main problem facing Cu- and Ag-based chalcogenides for TE device applications is the migration of Cu and Ag ions into the electrodes under applied current (for cooling applications) or a large temperature gradient (for power generation) [23]. Regarding this problem, recently a few research groups reported on Cu-based chalcogenides. The thermal stability of Cu_2Se was recently modified by changing the Cu:Ag ratio or by doping with small quantities of In Refs. [24,25]. Besides, P. Qiu et al. proposed that electrically conducting interfaces can be used to block Cu diffusion [26]. However, there is no detailed report on the high temperature thermal stability of Ag_2Se in spite of extensive studies on the low temperature TE properties, reporting *ZT* values in the range of 0.1–1 in the past few years [27–31].

In this work, we report on both low and high temperature TE properties of bulk Ag_2Se with nano-grained Cu_2Se inclusions ((bulk Ag_2Se)$_{1-x}$(nano-Cu_2Se)$_x$; x = 0, 0.02 and 0.05). The thermal stability of the samples was also examined via heating microscopy, and the heat capacity as a function of temperature.

2. Experimental methods

2.1. Sample preparation

Bulk Ag_2Se was prepared by the conventional method of melting and annealing [32]. Nano-grained Cu_2Se powders (referred to as "nano-Cu_2Se powder" hereon) were prepared with a microwave assisted thermolysis presented in detail in our earlier work [33]. Obtained ingots of Ag_2Se were ground by hand into fine powder and mixed with nano-Cu_2Se powder in the ratio of 2% and 5% of mol of Ag_2Se. Powdering and mixing processes were carried out in a nitrogen-filled glove box. The mixtures were then loaded into agate jars containing agate milling balls at a 5:1 ball-to-powder mass ratio. The jars were sealed in nitrogen filled glove box to minimize oxygen contamination during the milling process. The sealed jars were mounted on a planetary ball mill (Optosense), and the powders were then mechanically alloyed for 1 h to obtain homogenous solid solutions. Finally, mixed powders were compacted with SPS under 50 MPa of pressure with 15 min holding time.

2.2. Structural characterization

Room temperature powder X-ray diffraction (PXRD) analysis was carried out with a Rigaku Ultima X-ray diffractometer equipped with graphite monochromated Cu Kα radiation, operating at 40 kV and 100 mA. Scanning electron microscopy with energy dispersive X-ray (SEM-EDX) analysis was performed via a Phenom ProX Scanning Electron Microscope. The thermal expansion of the samples was tested by using a Misura 3HSML heating microscope.

2.3. Transport property measurement

TE transport properties were evaluated from 5 K to 875 K. The Seebeck coefficient and thermal conductivity below ambient were collected

using longitudinal steady-state measurements in a homebuilt cryostat. Low temperature Hall effect data (2–300 K) were collected using Quantum Design Magnetic Property Measurement System (MPMS) connected to a Linear Research AC Resistance Bridge operating at 12 Hz. Both positive and negative magnetic fields of magnitude 0.5 T were used to correct for small probe misalignment. The sign of the Hall coefficient R_H determines the charge carrier type, while $n_H = (R_H{}^*e)^{-1}$ is the carrier concentration, with e the elementary charge, calculated from a single carrier model given the linear Hall signal with respect to applied field. The charge carrier mobility is calculated by $\mu_H = R_H{}^*\sigma$. The high temperature Seebeck coefficient and electrical conductivity measurements were performed by the commercially available ULVAC-Riko ZEM 3 M8 model apparatus. The total thermal conductivity κ was calculated according to $\kappa = D \cdot \rho \cdot C_p$, where D is the thermal diffusivity, C_p the heat capacity and ρ the bulk density. Thermal diffusivity was measured using the LFA1000 Laser Flash apparatus from Linseis company. Specific heat was measured by differential scanning calorimetry (PT1000 Linseis company), and density was obtained from the Archimedes' method. The typical error bar expected in the Seebeck coefficient and electrical conductivity is ±7%, while it is ±10% for thermal conductivity.

3. Results and discussion

3.1. Structural data

Fig. 1 shows the PXRD pattern obtained on $(Ag_2Se)_{1-x}$(nano-Cu_2Se)$_x$ samples, where x = 0, 0.02 and 0.05, at 300 K. The room temperature PXRD pattern of samples confirms the main phase of Ag_2Se space group $P2_12_12_1$ [19] orthorhombic (ICDD Card#: 96-223-0973) in all compounds that is consistent with previous reports [17,27,28]. Small quantities of the Cu_2Se phase were detected at 28° only in the 5 mol % nano-Cu_2Se (Card# 00-088-2043) included sample.

In order to further examine the phase composition of the samples, SEM-EDX analyses were conducted on the 5 mol% nano Cu_2Se included bulk Ag_2Se. Fig. 2 summarizes the results.

SEM-EDX analysis of $(Ag_2Se)_{0.95}$(nano-Cu_2Se)$_{0.05}$ shows that there are two phases of Ag_2Se (bright regions in Fig. 2(a)) and Cu_2Se (dark regions) in the compound, as already suggested by the PXRD. However, despite observing a small trace of the Cu_2Se phase in the PXRD pattern, the SEM-EDX map displays a large quantity of Cu_2Se in the compound. This might be due to an agglomeration of Cu_2Se likely due to inhomogeneous distribution of nano-Cu_2Se in the Ag_2Se matrix.

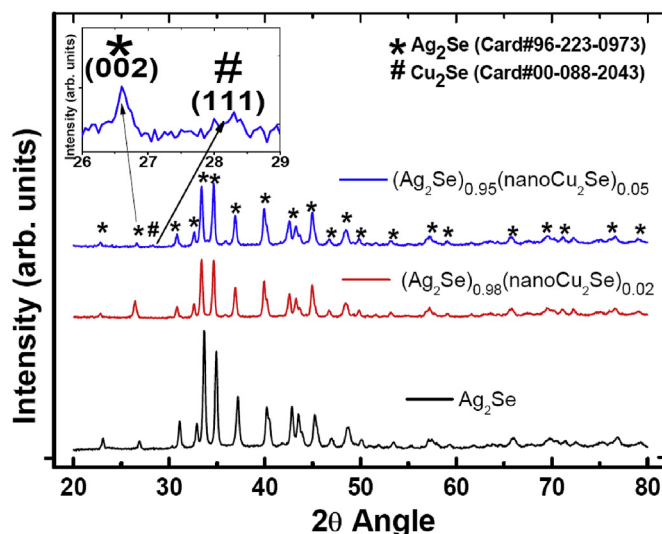Despite attractive attributes, such as low toxicity and ease of

Fig. 1. PXRD pattern of $(Ag_2Se)_{1-x}(Cu_2Se)_x$ samples, where x = 0, 0.02 and 0.05.
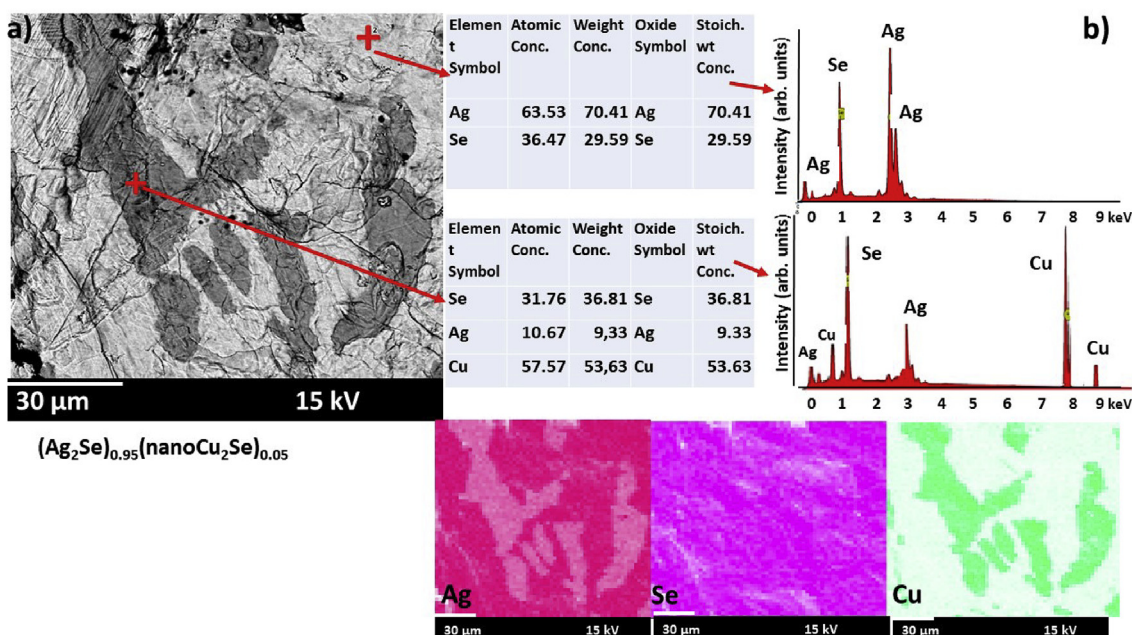
Fig. 2. SEM micrograph (a) and EDX elemental analysis (b) of $(Ag_2Se)_{0.95}(Cu_2Se)_{0.05}$ sample showing the composite nature of the material.
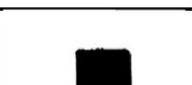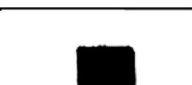

Fig. 3. Hot stage microscopy images illustrating the temperature dependence of the thermal expansion (surface deformation in %) of $(Ag_2Se)_{1-x}(Cu_2Se)_x$ samples, where x = 0, 0.02 and 0.05.

synthesis, the deployment of Ag_2Se and Cu_2Se into working TE devices is still problematic due to structural and chemical instability issues. In order to analyze surface deformation of the composites in this study, the thermal expansion of the samples were analyzed with heating microscopy. Obtained results are presented in Fig. 3.

Thermal expansion (%) in pure Ag_2Se reaches ~9% at 673 K while it is much less at 473 K and 573 K. The sudden change of shape and thermal expansion of Ag_2Se at 673 K might be due to decomposition (Se evaporation) above 600 K that softens the material. Contrary to bulk Ag_2Se, nano-Cu_2Se included samples show ~4% thermal expansion at 673 K, exhibiting greater thermal stability than the bulk Ag_2Se [37]. Increasing thermal expansion with increasing temperature for all samples is likely due to increase in the size of the unit-cell as alpha-beta transition

completes [34]. The increasing thermal stability of Ag_2Se with nano-Cu_2Se inclusion might be due to partly diffusion of Cu ions into Ag_2Se and acting like Ag^+ mobility disruption center [25,35].

In order to further understand the dependence of the thermal stability of Ag_2Se on the amount of the nano-Cu_2Se, the temperature dependence of the heat capacity was examined (see Fig. 4).

Heat capacity measurements are a useful, indirect yet sensitive method to detect structural changes in a material. From Fig. 4, all samples reveal a clear signature of a phase transition between 400 and 450 K, which is the well-known α-β structural transition in Ag_2Se and Cu_2Se materials as described earlier [27,32]. Upon nano-Cu_2Se inclusion, the transition shifts by a few degrees to lower temperature. The phase transition temperature is strongly dependent on the defect structure of a
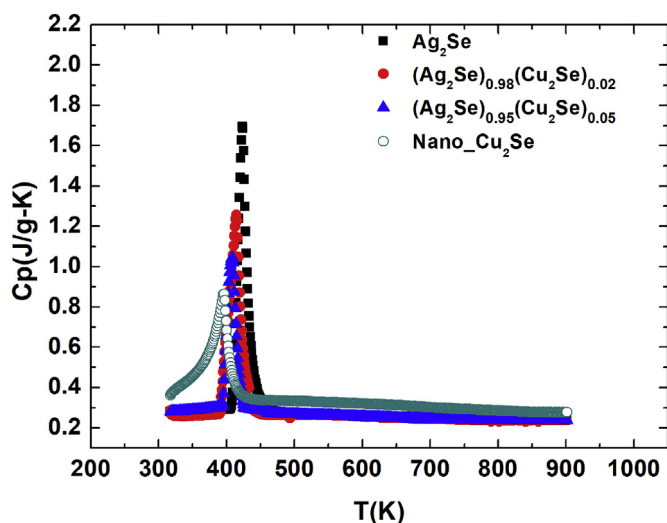
Fig. 4. Temperature dependence of heat capacity for $(Ag_2Se)_{1-x}(nano\text{-}Cu_2Se)_x$ and nano Cu_2Se samples, where $x = 0$, 0.02 and 0.05.

material as well as its phase composition [36]. Therefore, the shift of the phase transition temperature might due to increasing number of Ag vacancies in the Ag_2Se matrix or potentially the occurrence of the same structural transition in the Cu_2Se secondary phase at lower temperatures. The intensity of a phase transition peak is related to energy difference between the two phases and also reflect the chemical stability of compound [37]. In other words, compounds that have small peak intensity in the heat capacity are more stable thermally and chemically in comparison to compounds with higher peak intensity. As can be clearly seen in Fig. 4, the peak intensity of the phase transition in the samples of this

study decreases with increasing nano-Cu_2Se inclusion. Therefore, both thermal expansion (Fig. 3) and heat capacity versus temperature measurements (Fig. 4) confirm the thermal stability of the compounds is enhanced with the nano inclusions.

3.2. Transport data

The temperature-dependent Hall coefficient, carrier density and mobility of nano-Cu_2Se included Ag_2Se samples are presented in Fig. 5.

Low temperature thermoelectric properties of Ag_2Se were studied in detail by several groups [27,28,37–39]. However, the different reported values of transport properties indicate that they are very sensitive to sample preparation process, excess of Ag/Se and doping. In order to determine the carrier type in the composite, the Hall coefficient measurement was performed. The negative sign of the Hall coefficient indicates that electrons are the main charge carriers in all samples. Fig. 5 (b) shows temperature dependence of the carrier density of the samples. With increasing nano-Cu_2Se inclusion, the electron concentration is enhanced, likely due to the diffusion of some Cu ions into the Ag_2Se structure that serve to donate electrons. Dependence of charge carrier density on temperature (Fig. 5(b)) is nearly flat (extrinsic conduction) for the composite with 2 mol% nano-Cu_2Se inclusion while with 5 mol% inclusion a thermally activated behavior is observed above 200 K that indicates some form of donor state. Carrier mobility was calculated via $\mu_H = R_H * \sigma$. Carrier mobility (shown in Fig. 5(c)) decreases with increasing content of nano-Cu_2Se likely due to the increase in the carrier density (electron-electron interaction) or due to scattering of charge carrier on interfaces and grains that formed from the nano-Cu_2Se substitution. Fig. 5(d) displays the logarithm of the low temperature mobility plotted against log temperature with power-law exponents indicated for the samples to emphasize the particular scattering mechanism governing the $\mu_H \propto T^r$ relation. The data suggest that carrier-charged defect

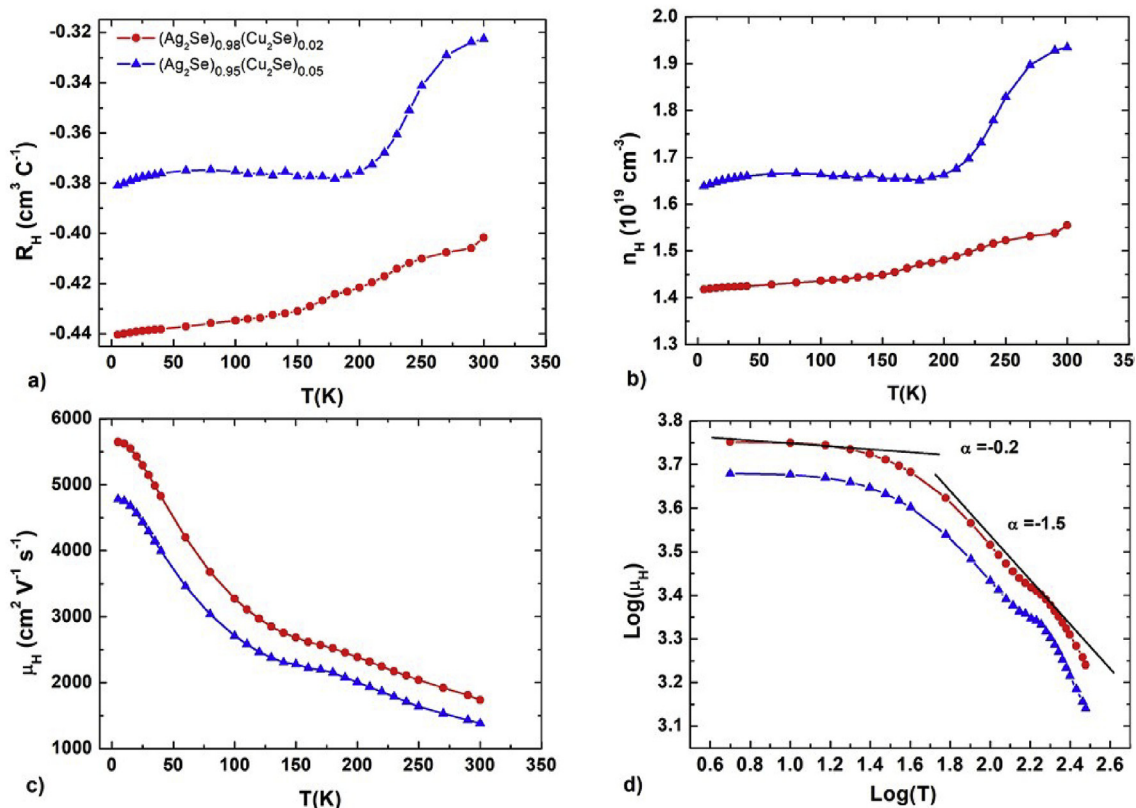**Fig. 5.** Temperature-dependent a) Hall coefficient, b) carrier density, c) carrier mobility and d) log mobility vs log temperature for $(Ag_2Se)_{1-x}(Cu_2Se)_x$ samples, where x is 0.02 and 0.05.

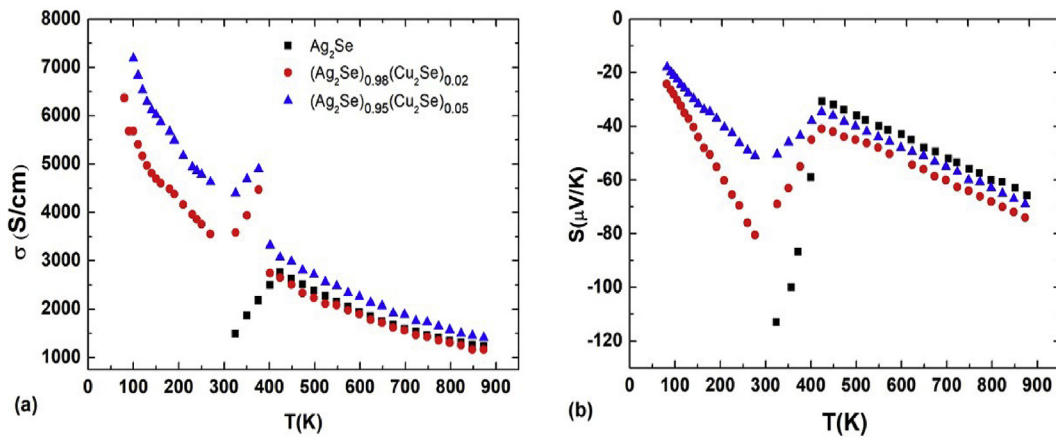**Fig. 6.** Temperature-dependent electrical conductivity (a) and Seebeck coefficient (b) of $(Ag_2Se)_{1-x}(Cu_2Se)_x$ samples, where x = 0, 0.02 and 0.05.

(5–50 K) then carrier-acoustic phonon scattering (50–300 K) is dominant in the samples.

Electrical conductivity and Seebeck coefficient as a function of temperature for all samples are presented in Fig. 6. Because of the greater number of charge carriers, the electrical conductivity of the samples with higher nano-Cu_2Se content is improved. Curiously, the room temperature electrical conductivity values of the samples (Fig. 6(a)) are quite different (1480 S/cm, 3580 S/cm, 4319 S/cm for Ag_2Se, 2%nanoCu_2Se and 5% nano-Cu_2Se included samples respectively), whereas above the phase transition, the values are much closer (2620 S/cm, 2502 S/cm, 2981 S/cm for Ag_2Se, 2%nanoCu_2Se and 5%nanoCu_2Se included samples respectively). This might be due to a matching of the crystal structures of Cu_2Se and Ag_2Se after the phase transition. In other words, the crystal structure of nano-Cu_2Se is monoclinic before the phase transition and turns into a cubic structure after the phase transition [31,32]. Similarly, Ag_2Se shows an orthorhombic crystal structure before the phase transition and then turns into cubic structure after the phase transition [27,30]. Therefore, both compounds have a nearly identical crystal structure above the phase transition temperature, leading to a similar environment in which the electrons move leading to similar values of σ. As is typical for degenerate semiconductors, the Seebeck coefficient is inversely proportional with the electrical conductivity for all samples. Additionally, all materials show negative values of the Seebeck coefficient that indicates that electrons are dominant carriers in all samples, which is consistent with Hall coefficient measurements (Fig. 5(a)).

Total thermal conductivity (Fig. 7(a)) was suppressed with the inclusion of 5 mol% nano-Cu_2Se, despite the increase in the electrical conductivity. The 2 mol% nano-Cu_2Se included sample shows very similar values to Ag_2Se.

We used the Wiedemann-Franz law to calculate the lattice contribution to the thermal conductivity of $(Ag_2Se)_{1-x}(Cu_2Se)_x$ samples by subtracting the electronic term ($\kappa_e = L\sigma T$ where L, σ and T are the Lorenz number, electrical conductivity and absolute temperature, respectively) from the total thermal conductivity. The Lorenz number for all compounds was calculated by using the following equations;

$$L = \left(\frac{k_B}{e}\right)^2 \left[\frac{(r+7/2)F_{r+5/2}(\xi)}{(r+3/2)F_{r+1/2}(\xi)} - \left(\frac{(r+5/2)F_{r+3/2}(\xi)}{(r+3/2)F_{r+1/2}(\xi)}\right)^2\right] \quad (1)$$

where r is the scattering parameter, k_B the Boltzmann constant, e is the electron charge, and $F_n(\xi)$ is the Fermi integral given by

$$F_n(\xi) = \int_0^\infty \frac{\chi^n}{1 + e^{\chi-\xi}} d\chi \quad (2)$$

Here ξ is the reduced Fermi energy that can be calculated from the Seebeck coefficient S and the scattering parameter r according to

$$S = \pm\frac{k_B}{e} \frac{(r+5/2)F_{r+3/2}(\xi)}{(r+3/2)F_{r+1/2}(\xi)} - \xi \quad (3)$$

We assumed the system to be highly degenerate and scattering dominated by acoustic phonons [32]. The calculated Lorenz numbers for Ag_2Se, $(Ag_2Se)_{0.98}(Cu_2Se)_{0.02}$, and $(Ag_2Se)_{0.95}(Cu_2Se)_{0.05}$ samples, are 1.87×10^{-8} V^2/K^2, 2.01×10^{-8} V^2/K^2, and 2.05×10^{-8} V^2/K^2 respectively. The calculated lattice thermal conductivities (κ_L) are shown in Fig. 7(b). Unrealistic negative values of the lattice thermal conductivity in 5%mol nano Cu_2Se resulted from our calculations so they are not shown here. Although one reason for the drastically reduced lattice
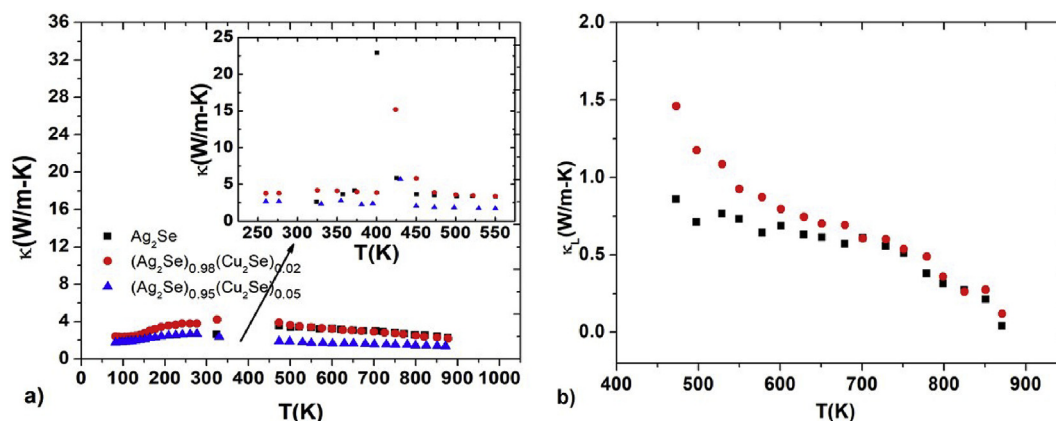

Fig. 7. Total thermal conductivity (a) and lattice part of the thermal conductivity (b) versus temperature for $(Ag_2Se)_{1-x}(Cu_2Se)_x$ samples, where x = 0, 0.02 and 0.05. The x = 0 sample is not included in (b) due to the unphysical negative values of the lattice thermal conductivity, as explained in the text.

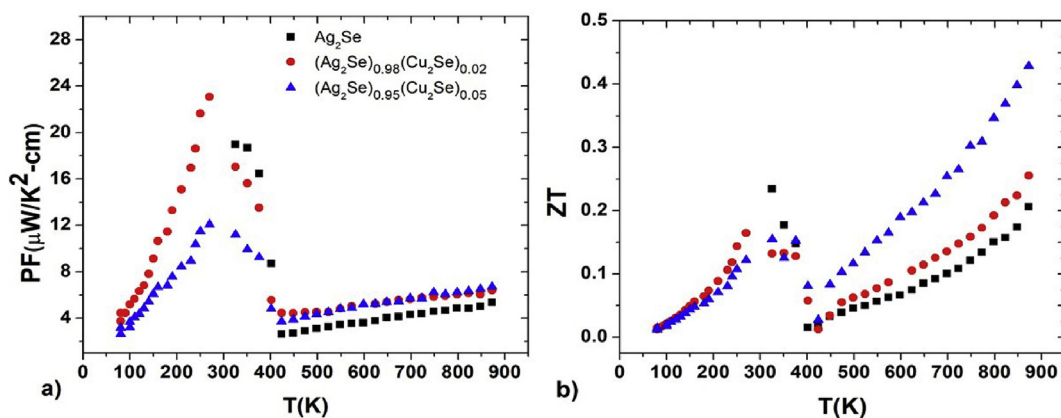**Fig. 8.** (a) Thermoelectric figure of merit (ZT) and (b) Power factor versus temperature for $(Ag_2Se)_{1-x}(Cu_2Se)_x$ samples, where x = 0, 0.02 and 0.05.

thermal conductivity is the scattering of heat carrying phonons on the interface and grain boundary that form via nano phases, the negative values might be due to softening lattice vibration in this compound as Olvera et al. indicated in their work [25]. Another possible reason for observing negative values is that the laser flash technique may not be entirely accurate with materials that are somewhat thermally unstable, causing an underestimation of the total thermal conductivity.

The combination of high Seebeck coefficient and high electrical conductivity leads to a maximum power factor of 24 µW/(K^2-cm) at room temperature for the sample with 2 mol% nano-Cu_2Se inclusion.

The dimensionless TE figure of merit, *ZT*, reaches ~0.25 at 300 K for bulk Ag_2Se and ~0.45 at 875 K for the 5 mol% nano-Cu_2Se included compound, due to lower thermal conductivity and a relatively high power factor (Fig. 8).

4. Conclusion

$(Ag_2Se)_{1-x}(Cu_2Se)_x$ solid solutions, where x = 0, 0.02 and 0.05, were prepared by a two-step process in which the bulk Ag_2Se was melted and annealed, while the nano-grained Cu_2Se powders were derived from a microwave assisted synthetic procedure. The two compounds were mixed via ball milling then densified with the spark plasma sintering method. PXRD and SEM-EDX patterns indicate that there are two phases in microstructure, which are Ag_2Se and Cu_2Se. Thermal expansion and thermodynamic stability of samples were tested with Heating microscopy and heat capacity measurement. Both analyses revealed that nano-Cu_2Se increases the thermal stability of compounds. The Hall effect measurement and electrical conductivity demonstrated a positive trend in the electrical conductivity with increasing nano inclusion due to higher resultant carrier density. Total thermal conductivity decreases and *ZT* values increase with nano-Cu_2Se inclusion. It is concluded that all transport and structural data indicate that nano Cu_2Se inclusions improve TE properties and thermal stability of Ag_2Se. Synthesizing nano grained powder of Ag_2Se and its effect on transport properties of Cu_2Se will be a part of our future work.

Acknowledgments

References

[1] EIA-MER. https://www.eia.gov/totalenergy/data/monthly/.

[2] C. Uher, Material Aspect of Thermoelectricity, CRC Press, Taylor & Francis, Boca Raton, FL, 2016.

[3] G. Tan, L.-D. Zhao, M. Kanatzidis, Chem. Rev. 16 (2016) 12123.

[4] G.A. Slack, in: D.M. Rowe (Ed.), CRC Handbook of Thermoelectricity, CRC Press, Boca Raton, 1995, p. 407.

[5] M. Beekman, D.T. Morelli, G.S. Nolas, Nat. Mater. 14 (2015) 1182.

[6] K.F. Hsu, S. Loo, F. Guo, W. Chen, J.S. Dyck, C. Uher, T. Hogan, E.K. Polychroniadis, M.G. Kanatzidis, Science 303 (2004) 818.

[7] B. Poudel, Q. Hao, Y. Ma, Y. Lan, A. Minnich, B. Yu, X. Yan, D. Wang, A. Muto, D. Vashaee, X. Chen, J. Liu, M.S. Dresselhaus, G. Chen, Z. Ren, Science 320 (2008) 634.

[8] J.P. Heremans, V. Jovovic, E.S. Toberer, A. Saramat, K. Kurosaki, A. Charoenphakdee, S. Yamanaka, G.J. Snyder, Science 321 (2008) 554.

[9] Y.Z. Pei, X. Shi, A. LaLonde, H. Wang, L.D. Chen, G.J. Snyder, Nature 473 (2011) 66.

[10] W. Liu, X. Tan, K. Yin, H. Liu, X. Tang, J. Shi, Q. Zhang, C. Uher, Phys. Rev. Lett. 108 (2011) 166601.

[11] D.T. Morelli, V. Jovovic, J.P. Heremans, Phys. Rev. Lett. 101 (2008), 035901.

[12] H. Li, X. Tang, Q. Zhang, C. Uher, Appl. Phys. Lett. 93 (2009), 252109.

[13] H. Liu, X. Shi, F. Xu, L. Zhang, W. Zhang, L. Chen, Q. Li, C. Uher, T. Day, G.J. Snyder, Nat. Mater. 11 (2012) 422.

[14] B. Yu, W. Liu, S. Chen, H. Wang, H. Wang, G. Chen, Z. Ren, Nano Energy 1 (2012) 472.

[15] K. Peng, B. Zhang, H. Wu, X. Cao, A. Li, D. Yang, X. Lu, G. Wang, X. Han, C. Uher, X. Zhou, Mater. Today 21 (2018) 501.

[16] A.D. LaLonde, Y. Pei, H. Wang, G.J. Snyder, Mater. Today 14 (11) (2011) 526–532.

[17] W. Mi, P. Qiu, T. Zhang, Y. Lv, X. Shi, L. Chen, Appl. Phys. Lett. 104 (2014), 133903.

[18] C. Lee, Y. Park, H. Hashimoto, J. Appl. Phys. 101 (2007), 024920.

[19] X. Zhang, C.L. Zhang, S. Lin, H. Lu, Y. Pei, S. Jia, J. Appl. Phys. 119 (2016), 135101.

[20] Y. Yang, D. Pan, Z. Zhang, T. Chen, H. Xie, J. Gao, X. Guo, J. Alloys Compd. 766 (2018) 925.

[21] K. Zhang, J. Feng, H. Liu, Chem. Phys. Lett. 706 (2018) 388.

[22] S. Yang, K. Cho, Y. Park, S. Kim, Nano Energy 49 (2018) 333.

[23] T.P. Bailey, C. Uher, Curr. Opin. Green Sustain. Chem. 4 (2017) 58.

[24] A. Olvera, T.P. Bailey, C. Uher, P.F.P. Poudeu, J. Mater. Chem. A 6 (2018) 6997.

[25] A. Olvera, N. A Moroz, P. Sahoo, P. Ren, T. P Bailey, A. Page, C. Uher, P.F.P. Poudeu, Energy Environ. Sci. 10 (2017) 1668.

[26] P. Qiu, M.T. Agne, Y. Liu, Y. Zhu, H. Chen, T. Mao, J. Yang, W. Zhang, S.M. Haile, J. Janek, C. Uher, X. Shi, L. Chen, G.J. Snyder, Nat. Commun. 2018 (2019) 9.

[27] M. Ferhat, J. Nagao, J. Appl. Phys. 88 (2000) 813–816.

[28] F. Aliev, M. Jafarov, V. Eminova, Atomic structure and nonelectronic properties of semiconductors 43 (2009) 1013–1015.

[29] T. Sakuma, K. Iida, K. Honma, H. Okazaki, J. Phys. Soc. Jpn. 43 (1977) 538–543.

[30] F.F. Aliev, M.B. Jafarov, V.I. Eminova, Semiconductors 43 (2009) 977–979.

[31] W. Mi, P. Qiu, T. Zhang, Y. Lv, X. Shi, L. Chen, Appl. Phys. Lett. 104 (2014), 133903.

[32] S. Ballikaya, H. Chi, J.R. Salvador, C. Uher, J. Mater. Chem. A 1 (2013) 12478.

[33] M.Y. Tafti, S. Ballikaya, et al., RSC Adv. 6 (2016) 111457.

[34] L.D. Gulay, M. Daszkiewicz, O.M. Strok, A. Pietraszko, Chem. Met. Alloys 4 (2001) 200.

[35] P. Qiu, T. Zhang, Y. Qiu, X. Shi, L. Chen, Energy Environ. Sci. 7 (2014) 4000–4006.

[36] X. Xing-Xing, X. Wen-Jei, T. Xin-Feng, Z. Qing, Chin. Phys. B 20 (2011), 087201.

[37] D. Brown, Enhanced Thermoelectric Performance at the Superionic Phase Transitions of Mixed Ion-Electron Conducting Materials, Dissertation (Ph.D.), California Institute of Technology, 2015, https://doi.org/10.7907/Z9B56GNM.

[38] H. Wang, W. Chu, D. Wang, W. Mao, W. Pan, Y. Guo, Y. Xiong, H. Jin, J. Electron. Mater. 40 (2011) 624.

[39] M.B. Jafarov, Semiconductors 44 (2010) 1280.